 Bull. Chem. Soc. Jpn. Vol. 82, No. 8, 953–962 (2009)

Quasi-Classical Trajectory Dynamics Study on the Reaction of H with HO_2

Seyed Hosein Mousavipour* and Issa Yousefiasl

Department of Chemistry, College of Sciences, Shiraz University, Shiraz 71454, Iran

Received November 6, 2008; E-mail: mousavi@susc.ac.ir

Quasi-classical trajectory (QCT) simulations, based on our previously reported PES data (*Bull. Chem. Soc. Jpn.* **2007**, *80*, 1901) were carried out to study the dynamics of the lowest singlet potential energy surface of $H + HO_2$ reaction. The surface consists of two potential wells due to formation of water oxide (H_2OO^*) and hydrogen peroxide ($HOOH^*$). A detailed consideration of the dynamics of the intermediates H_2OO^* and $HOOH^*$ reveals that water oxide and hydrogen peroxide geometries, largely undergo asymmetric or symmetric stretching like motions until they dissociate. The QCT calculations revealed that the reaction is very sensitive to the vibrational excitation of HO_2. In general, QCT integral, reactive reaction cross-sections and rate constants are found to be in good agreement with their QM and experimental counterparts, indicating that, for this system, the motion of the nuclei during reactive encounters is largely classical and that quantum effects, such as tunneling, play a relatively minor role in the overall dynamics. The intramolecular vibrational energy redistribution (IVR) involving excitation of the OH and OO bonds in HOOH is investigated. The calculated IVR time constants describing energy flow out of the OH and OO stretching modes are reported. It is found that calculated IVR time constants decrease exponentially with increasing the amount of energy put in the relevant modes.

Hydrogen–oxygen systems play important roles in the chemistry of atmosphere and combustion.[1] Reaction of hydrogen atoms with hydroperoxyl radical HO_2 and its reverse has attracted the attention of many researchers.[2–23] Recently, the kinetics of gas-phase reaction of $H + HO_2$ on both singlet and triplet surfaces is studied in our group.[23] The following mechanism is suggested for this system (Scheme 1).

Early work on this system has mostly been concerned about the branching ratios of different reaction paths to form $H_2 + O_2$, $H_2O + O$, or 2OH with brief attention to the mechanism. In 1972 Westenberg and DeHaas[2] have proposed three major paths for this system (formation of $H_2 + O_2$, $H_2O + O$, and 2OH) and determined the relative values of the rate of formation of these products to the value of disappearance rate of reactants as 0.62, 0.11, and 0.27, respectively, at 298 K, while Sridharan et al.[4] reported values of 0.09 ± 0.045, 0.04 ± 0.02, and 0.87 ± 0.04, respectively, at 296 ± 2 K. Keyser[5] has determined the branching ratios to be 0.08 ± 0.04, 0.02 ± 0.02, and 0.90 ± 0.04 for the formation of $H_2 + O_2$, $H_2O + O$, and 2OH, respectively, in agreement with those reported by Boutalib et al.[6] that have shown hydrogen abstraction channels to form $H_2 + O_2$ to be more

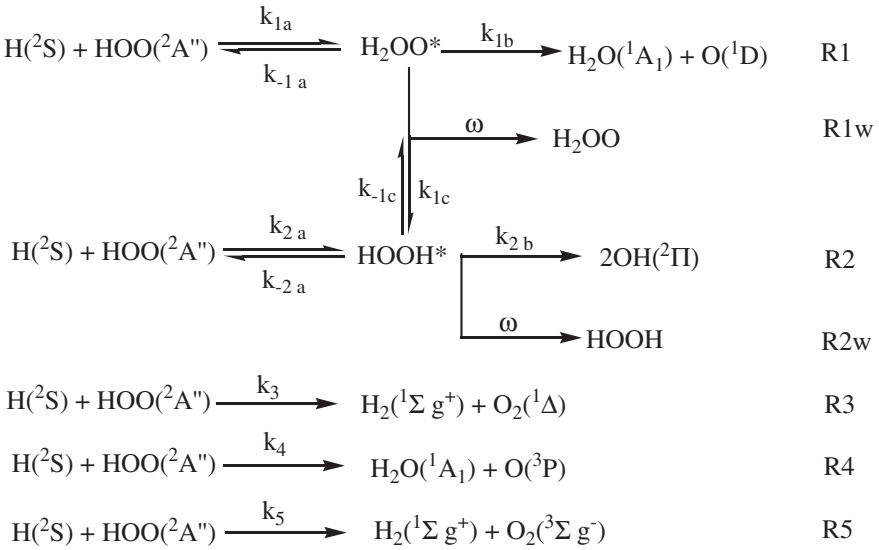

Scheme 1.

Published on the web August 7, 2009; doi:10.1246/bcsj.82.953

plausible than disproportionation reaction to form $H_2O + O$. Baldwin et al.[3] have reported the ratio of the rate constants for the formation of OH to $H_2 + O_2$ as 5.9 at 773 K and over a pressure range of 10.5–24.8 kPa. They were not able to distinguish between reaction path for the formation of OH radicals and reaction path for the formation of $H_2O + O$.

In the previous studies the role of formation of water oxide on the kinetics of this system is not considered except in Ref. 23. One interesting aspect in this system is the presence of transient species water oxide, H_2OO. Some researchers have reported the possibility of existing water oxide as a short lived species in gas-phase and also in liquid phase, which undergoes isomerization according to step k_{1c} or dissociates to $H_2O + O$ according to step k_{1b} in our proposed mechanism.[9]

It has been proposed by Schröder et al.[9f] that water oxide can be formed as a transient species on the singlet potential energy surface in the $H_2 + O_2$ system. To the best of our knowledge, their work is the first experimental report of the existence of water oxide. According to their results, singlet water oxide is 196.5 kJ mol^{-1} less stable than hydrogen peroxide. Sayós et al.,[9i] in a quasiclassical trajectory study on the reaction of $O(^1D) + H_2O(^1A_1)$, have shown that water oxide is 211.9 kJ mol^{-1} less stable than hydrogen peroxide at UMP2 level of theory. Filatov et al.[9j] have studied the reason for the kinetic stability of the $H_2 + O_2$ mixture. They have reported that water oxide is 209.4 kJ mol^{-1} less stable than hydrogen peroxide at the MR-(S)DCI/cc-pVTZ level.

Toohey and Anderson,[10] in a theoretical study on the reaction of some small radicals with HO_2, have considered a transition structure of HHOO species with an imaginary frequency and a barrier height of 23.0 kJ mol^{-1} relative to the total energy of $H + HO_2$ at the UMP2/6-31G** level. It seems they have only considered the structure of H–H–O=O instead of considering the structure of water oxide. This energized intermediate has been reported to exist with a short lifetime which dissociates to $H_2O + O(^1D)$ according to channel R1 or undergoes isomerization to produce energized HOOH*, which then dissociates to $OH(^2\Pi)$ via channel R2 or undergoes stabilization according to R2w. The produced energized hydrogen peroxide in channel R2 undergoes dissociation to produce hydroxyl radicals unless stabilized by collision with the other species, R2w.

This system consisted of multichannels with two deep potential energy wells on a singlet surface. The singlet potential energy surface consisted of three paths, which might be simplified as shown in Scheme 2. Reactions R1 and R2 proceed through deep potential wells belonging to H_2OO* and HOOH* as shown in Figure 1.[23] Understanding the dynamics of chemical reactions consisting of multichannels with deep potential energy wells is of great important. To the best of our knowledge, no experimental data are reported on whether reactions R1 and R2 are affected by slow intramolecular vibrational energy redistribution (IVR). IVR enables energy in the reaction coordinate to be redistributed, which causes higher probability of collisional deactivation relative to the rate of dissociation.

Using quasi-classical trajectory (QCT) calculations make it possible to investigate the reaction mechanism more clearly, view the transition state behavior (where chemical bonds are broken and formed), and examine the possible presence of resonances in the deep potential intermediate. QCT calculations enables one to obtain reaction probabilities and cross sections for fundamental reactions and to simulate strongly non-equilibrium flows. The title mentioned system consisted of at least 5 different channels on both singlet and triplet potential with main products $H_2 + O_2$, OH, and $H_2O + O$ in singlet or triplet states.[23] The rate of decomposition of the two chemically activated intermediates is much faster than the rate of stabilization process by collisional deactivation.[23] One interesting aspect for dynamic study is to verify whether the reactive system becomes temporarily trapped in one of these minima, forming a reaction intermediate. Furthermore, if the intermediate is trapped for a sufficiently long period of time, energy may become randomized amongst its vibrational degrees of freedom, giving rise to a statistical intermediate. QCT simulations may be used to probe the behavior of the intermediates regarding the classical or non-classical behavior of these intermediates in the title mentioned system.

It was the purpose of the present study to investigate the effect of relative translational energy and temperature, and initial vibrational excitation of HO_2 on the reactive cross section and reaction probability. We were also interested in examining the lifetime of the energized intermediates H_2OO* and HOOH* as a function of translational energy and also to calculate the IVR time constants of excited OH and OO bonds in HOOH intermediate.

Given that tunneling is neglected by QCT methods, it would be necessary to consider this phenomenon by comparing the QCT results of reaction R3 with the experimental and MO calculations results.

$HO_2\,(^2A'')(\upsilon 00) + H(^2S) \rightarrow H_2OO^* \rightarrow H_2O(^1A_1) + O(^1D)$ R1

$HO_2\,(^2A'')(\upsilon 00) + H(^2S) \rightarrow HOOH^* \rightarrow 2\,OH(^2\Pi)$ R2

$HO_2\,(^2A'')(00\upsilon) + H(^2S) \rightarrow O_2(^1\Delta) + H_2(^1\Sigma_g^+)$ R3

Scheme 2.

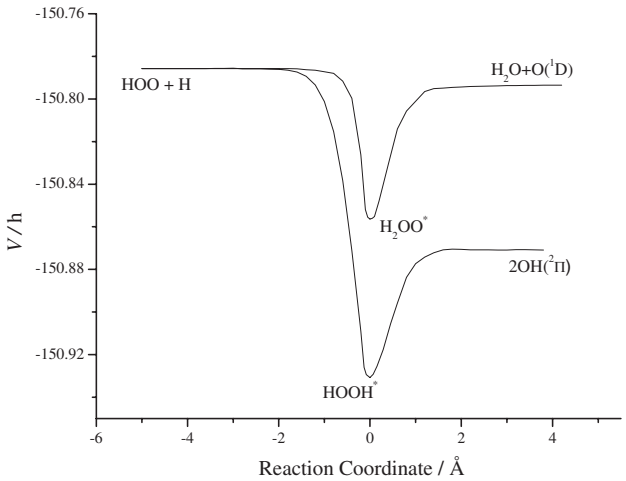

Figure 1. Vibrationally adiabatic ground state potential energy surface for reactions R1 and R2.

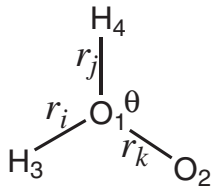

Scheme 3.

Theoretical Background

Intramolecular Potential. The QCT calculations are carried out by means of a modified version of the VENUS96[24] code in which the potential energy is formulated according to the curvilinear internal coordinates and then transformed to a Cartesian coordinate frame. The outcome of this procedure is a Hamiltonian that does not neglect terms in the kinetic energy expression.[25] The PES for this system was constructed by starting with 6 Å initial separations of H and HO_2. A simple valence force field, consisting of Morse oscillators and harmonic bends and torsion, was used to describe the overall potential energy of the system.

$$V_{\text{int}} = \sum_i V_{\text{stretch}} + \sum_i V_{\text{bend}} + \sum_i V_{\text{torsion}} \quad (1)$$

The spectator coordinates in this system were taken as distances (r) between different atoms as H···O or O···O, bends as H–O–H or O–O–H, and torsion as H–O–O–H. A Morse function provides a reasonable representation for stretching modes. The ab initio stretching potential was fitted by Morse function and two switching functions. We added switching functions to the stretching function in a similar fashion as suggested by Doubleday et al.[26] to turn on and off the reactant, product and the region between these extreme points. The switching functions $S(j)$ and $S(k)$ are used to optimize the force constants in the Morse stretches and harmonic bends.

$$V_i = D_i\{1 - \exp[-\beta_i(r_i - r_i{}^0)]\}^2 \times S(j)S(k) \quad (2)$$

where r_i is the bond length of the i-th bond and r_i^0 is the corresponding equilibrium distance. The switching function is defined as;

$$S(j) = \exp[-C_1(r_j - r_j{}^0)^2] \quad (3)$$

The same equation is true for $S(k)$. For instance, as shown in Scheme 3, the strength of H_3–O_1 bond changes by approaching H_4 to O_1.

A harmonic bend model was used to represent the dependency of potential energy as a function of different bending motions.

$$V_{\text{bend}} = 1/2F_{\theta_i}(\theta_i - \theta_i{}^0)^2 \quad (4)$$

where

$$F_{\theta_i} = F_{\theta_i}{}^0 S(j)S(k) \quad (5)$$

where θ_i is the i-th harmonic bend angle defined by bonds r_j and r_k, where θ_i^0 is the corresponding equilibrium angle.

The dependency of the potential energy to the torsion was calculated as

$$V_{\text{torsion}} = 0.5F_\varphi[1 + \cos(n\varphi)] \quad (6)$$

The singlet potential energy surface from Ref. 23 was used to fit and calculate the parameters in the analytical potential. The initial estimates for the Morse potential parameters (D and β), force constants, and torsion barrier heights were estimated from harmonic frequencies and bond dissociation energies for water oxide and hydrogen peroxide from the ab initio calculations at the CCSD level reported in Ref. 23. The optimum parameters of the potential function are listed in Table 1. The atom numbering is shown in Scheme 3. The equilibrium geometry of HO_2, H_2OO, and HOOH calculated from the analytical PES were in good agreement with the ab initio results. The maximum errors in bond distances and angles are only <0.06 Å and $<1.2°$, respectively.

Table 1. Potential Energy Surface Parameters[a)]

Parameters	Value	Parameters	Value
R(OO)/Å	1.32	β(OH)/Å^{-1}	2.3
R(OH)/Å	0.96	β(HH)/Å^{-1}	1.9
R(HH)/Å	0.74	θ(OOH)/°	102.2
$C_{2,3}$/Å^{-2}	5.5	θ(HOH)/°	106.7
$C_{3,4}$/Å^{-2}	12.5	φ(HOOH)/°	120.3
$C_{1,4}$/Å^{-2}	12.5	F(OOH)/mdyn Å rad^{-2}	0.50
$C_{1,2}$/Å^{-2}	6.5	F(HOH)/mdyn Å rad^{-2}	0.55
D_e(OO)/kJ mol^{-1}	489.1	F((HOOH)/mdyn Å rad^{-2}	0.08
D_e(OH)/kJ mol^{-1}	443.1	$C_{1,2,4}$/Å^{-2}	1.2
D_e(HH)/kJ mol^{-1}	455.6	$C_{2,1,3}$/Å^{-2}	1.2
β(OO)/Å^{-1}	2.7	$C_{4,2,3}$/Å^{-2}	1.2

a) Atom numbering is described in Scheme 3.

Details of Trajectory Calculations. The general chemical dynamics code VENUS96 was used to sample the reactant initial quasi-classical states and to integrate the classical equations of motion. In developing the model PES, we used a generalized Morse function, one of the built-in functions in VENUS, to model the stretching modes, the switching functions and its derivatives are added to the code.

Batches of 500–2000 trajectory have been run at a variety of collision energies, translational temperature, and initial vibrational states of HO_2 reactant. Calculations have been done for an atom tri-atom system with relative translational energies over the range of 6.3 to 83.6 kJ mol^{-1}, translational temperature from 300 to 1200 K, and initial HO_2 vibrational states from $\nu = 0$ to $\nu = 2$ for the corresponding mode in each reaction path. The initial rotational energies of the reactants are chosen from thermal distributions. The rotational energy about each principal axis of inertia of HO_2 has been taken as $K_BT/2$. The rotational temperature has been set to be 300 K in trajectory calculations. This corresponds to an intermediate value in the range of temperatures $100 \leq T/\text{K} \leq 500$, the temperature range of interest for researchers in atmospheric chemistry and combustion processes. The initial conditions are summarized in Tables 2 and 3. The fixed normal mode sampling method has been chosen for calculations. The maximum value of the impact parameter (b_{max}) is determined empirically in order to include more than 95% of reactive b_{max} trajectories. The impact parameter varied from 0.6 to 3.7 Å and the initial distance between the two reactant species has been fixed at 6.0 Å such as to make the interaction there essentially negligible. A combined fourth-order Runge–Kutta and sixth-order Adams–Moulton algorithms were used with a time step of 0.25 fs, which gave a typical conservation of total energy better than 2 in 10^5.

From the calculated reactive cross sections and reaction probability the specific thermal rate constants were calculated according to eq 7.[27]

$$k(T) = \left(\frac{8k_BT}{\pi\mu}\right)^{1/2} \pi b_{\text{max}}^2 \left(\frac{N_r}{N}\right) g_e \quad (7)$$

Table 2. Reaction Cross Section and Number of Reactive Trajectories as a Function of Collision Energy and Initial Vibrational Quantum Numbers of HO_2 Reactant

E_{tr}/kJ mol^{-1}	$\nu(HO_2)$[a)]	b_{max}/Å	N_r	σ[b)]/Å^2
$HO_2 + H \rightarrow H_2OO^* \rightarrow H_2O + O$				
6.3	(0,0,0)	0.6	8	0.009
6.3	(1,0,0)	0.8	8	0.016
6.3	(2,0,0)	1.0	8	0.025
20.9	(0,0,0)	1.0	16	0.050
20.9	(1,0,0)	1.2	16	0.072
20.9	(2,0,0)	1.4	16	0.098
41.8	(0,0,0)	2.4	16	0.288
41.8	(1,0,0)	2.4	24	0.434
41.8	(2,0,0)	2.6	24	0.510
62.7	(0,0,0)	2.6	24	0.510
62.7	(1,0,0)	2.7	24	0.550
62.7	(2,0,0)	3.2	24	0.772
83.6	(0,0,0)	2.7	24	0.550
83.6	(1,0,0)	2.9	32	0.847
83.6	(2,0,0)	3.3	32	1.094
$HO_2 + H \rightarrow HOOH^* \rightarrow 2OH$				
6.3	(0,0,0)	0.6	40	0.041
6.3	(1,0,0)	0.8	48	0.096
6.3	(2,0,0)	1.0	40	0.126
20.9	(0,0,0)	1.2	56	0.253
20.9	(1,0,0)	1.3	56	0.297
20.9	(2,0,0)	1.5	80	0.565
41.8	(0,0,0)	2.3	24	0.398
41.8	(1,0,0)	2.4	24	0.434
41.8	(2,0,0)	2.5	32	0.628
62.7	(0,0,0)	3.0	16	0.452
62.7	(1,0,0)	3.2	16	0.514
62.7	(2,0,0)	3.4	24	0.871
83.6	(0,0,0)	3.2	16	0.514
83.6	(1,0,0)	3.4	24	0.871
83.6	(2,0,0)	3.6	24	0.976
$HO_2 + H \rightarrow O_2 + H_2$				
6.3	(0,0,0)			
6.3	(0,0,1)			
6.3	(0,0,2)			
20.9	(0,0,0)			
20.9	(0,0,1)			
20.9	(0,0,2)	2.0	1	0.009
41.8	(0,0,0)	2.4	2	0.025
41.8	(0,0,1)	2.6	2	0.048
41.8	(0,0,2)	2.8	4	0.133
62.7	(0,0,0)	2.6	4	0.234
62.7	(0,0,1)	2.8	6	0.348
62.7	(0,0,2)	3.0	9	0.462
83.6	(0,0,0)	3.0	10	0.320
83.6	(0,0,1)	3.2	15	0.515
83.6	(0,0,2)	3.3	25	0.555

a) Vibrational frequencies of HO_2 reactant (ν_1 is the O–O stretching, ν_2 is the bending, and ν_3 is the O–H stretching). b) $\sigma = \pi(b_{max})^2 P^r$.

Where μ is the reduced mass for the reactants, N_r is the number of trajectories that end in the formation of products for a specified reaction path, N is the total number of trajectories in the ensemble, and b_{max} is the maximum impact parameter. The ratio of N_r/N represents the reaction probability and g_e is the ratio of the electronic partition functions. To simplify the dynamics calculations, we assumed no electronic, spin–orbit, or Coriolis coupling between the surfaces. The collision impact parameter b was calculated according to $b = b_{max}R^{1/2}$, where R is a random number distributed uniformly between 0 and 1.

Table 3. Maximum Impact Parameter b_{max}, Reaction Cross Sections σ, Number of Reactive Trajectories N_r, and Rate Constant as a Function of Translational Temperature and Initial Vibrational Quantum Numbers of HO_2

T/K	$\nu(HO_2)$[a)]	b_{max}/Å	N_r	σ[b)]/Å^2	k/L mol^{-1} s^{-1}
$HO_2 + H \rightarrow H_2OO^* \rightarrow H_2O + O$					
300	(0,0,0)	3.5	8	0.308	0.80×10^{10}
300	(1,0,0)	4.0	8	0.402	1.04×10^{10}
300	(2,0,0)	4.6	8	0.528	1.38×10^{10}
600	(0,0,0)	3.4	8	0.288	1.20×10^{10}
600	(1,0,0)	3.6	16	0.648	2.68×10^{10}
600	(2,0,0)	4.2	16	0.800	3.31×10^{10}
1200	(0,0,0)	3.2	8	0.256	1.62×10^{10}
1200	(1,0,0)	3.4	16	0.581	3.68×10^{10}
1200	(2,0,0)	4.0	16	0.888	5.63×10^{10}
$HO_2 + H \rightarrow HOOH^* \rightarrow 2OH$					
300	(0,0,0)	3.5	16	0.610	2.16×10^{10}
300	(1,0,0)	3.8	16	0.728	2.56×10^{10}
300	(2,0,0)	4.2	16	0.886	6.24×10^{10}
600	(0,0,0)	3.3	24	0.821	5.26×10^{10}
600	(1,0,0)	3.6	24	0.976	6.25×10^{10}
600	(2,0,0)	3.7	24	1.032	6.61×10^{10}
1200	(0,0,0)	3.2	24	0.772	0.81×10^{11}
1200	(1,0,0)	3.5	32	1.230	1.30×10^{11}
1200	(2,0,0)	3.6	32	1.304	1.37×10^{11}
$HO_2 + H \rightarrow O_2 + H_2$					
300	(0,0,0)		0		
300	(0,0,1)		0		
300	(0,0,2)	5.0	1	0.002	2.31×10^{7}
600	(0,0,0)				
600	(0,0,1)	3.3	2	0.021	3.43×10^{8}
600	(0,0,2)	4.5	3	0.029	4.74×10^{8}
1200	(0,0,0)	2.8	2	0.040	9.24×10^{8}
1200	(0,0,1)	3.0	4	0.106	2.45×10^{8}
1200	(0,0,2)	3.5	5	0.210	4.86×10^{9}

a) Vibrational frequencies of HO_2 reactant (ν_1 is the O–O stretching, ν_2 is the bending, and ν_3 is the O–H stretching). b) $\sigma = \pi(b_{max})^2 P^r$.

The following expressions were used to calculate the ratio of the electronic partition functions of the products to the electronic partition function of the reactants for different paths at different temperatures.[28]

$$g_e(R1) = \frac{\left[5 + \left(3\exp\left(\frac{-227.6}{T}\right)\right) + \left(\exp\left(\frac{-325.9}{T}\right)\right)\right]}{4} \quad (8)$$

$$g_e(R2) = \frac{\left[2 + \left(2\exp\left(\frac{-201}{T}\right)\right)\right]^2}{4} \quad (9)$$

$$g_e(R3) = \frac{3}{4} \tag{10}$$

Here, we assumed in dynamic calculations including the electronic partition functions of the products instead of transition state electronic partition functions might be more applicable. The reason was due to our observations from the trajectories that it was not possible to determine the position of the saddle points or bottlenecks for the reactions and also there was not a unique path for the formation of each product.

Method for Determination of IVR Time Constant (τ_{IVR}). In the present work, QCT calculations were carried out with our modified version of VENUS96 to calculate the IVR time constants in energized intermediate HOOH*. The microcanonical initialization procedure in VENUS assumes that all vibrational degrees of freedom are separable harmonic oscillators. In VENUS code it is optional to monitor normal-mode or local-mode energies with time. It should be noted that the IVR time constant be significantly influenced by Coriolis coupling. Here we used the same method as described by Liu et al.[29] to calculate the IVR time constants. The harmonic vibrational energy in a bond can be monitored by looking at the mean-square displacement, $\langle(r - r^0)^2\rangle$ of the bond. The potential energy V and total energy E for a harmonic oscillator can be calculated as

$$V = \frac{1}{2} F(r - r^0)^2 = \frac{1}{2} FA^2 \sin^2(2\pi\nu t + \delta) \tag{11}$$

and

$$E = \frac{1}{2} FA^2 \tag{12}$$

Where F is the bond force constant, A is the vibrational amplitude, ν is the frequency, δ is a phase shift, and t is time. The mean-square displacement (MSD) is obtained by averaging over δ

$$\langle(r - r^0)^2\rangle_\delta = A^2 \frac{1}{2\pi} \int_0^{2\pi} \sin^2(2\pi\nu t + \delta)\mathrm{d}\delta = \frac{1}{2} A^2 \tag{13}$$

Therefore, the total energy of the harmonic oscillator is proportional to the MSD

$$E = F\langle(r - r^0)^2\rangle_\delta \tag{14}$$

In the trajectory calculations, the initial vibrational phases are scaled randomly, resulting in an average over phase shift δ. If the IVR takes place on a time scale that is much longer than the vibrational period, then the MSD will be time-dependent. The above relationships lead to the following expression for the ensemble average vibrational energy in the bond

$$\langle E(t)\rangle = \frac{F}{N} \sum_{i=1}^{N} [r_i(t) - r^0]^2 \tag{15}$$

Where N is the total number of trajectories and $r_i(t)$ is the instantaneous bond length at time t calculated during the i-th trajectory. The harmonic force constant was obtained from the Morse oscillator parameters

$$F = \left(\frac{\partial^2 V}{\partial r^2}\right)_{r^0} = 2b^2 D \tag{16}$$

Equation 15 might be used to obtain approximate energies of anharmonic O–H or O–O oscillators in hydrogen peroxide. Batches of 200 trajectories were calculated at each specified vibrational energy E_{OH} or E_{OO} using VENUS96 and eq 15 to determine the average approximate energies $\langle E_{OH}\rangle_{approx}$ and $\langle E_{OO}\rangle_{approx}$, separately. Each trajectory was numerically integrated for 3×10^5 time steps with a step size of 0.25 fs. During each trajectory, values of $(r_i(t) - r^0)^2$ were obtained and used to calculate $\langle E_{OH}\rangle_{approx}$ or $\langle E_{OO}\rangle_{approx}$ for the batch of trajectories by means of eqs 17 and 18, respectively.

$$\langle E_{OH}(t)\rangle_{approx} = \langle E_{OH}(0)\rangle \exp(-t/\tau_{IVR}) + \langle E_{OH}(\infty)\rangle \tag{17}$$

and

$$\langle E_{OO}(t)\rangle_{approx} = \langle E_{OO}(0)\rangle \exp(-t/\tau_{IVR}) + \langle E_{OO}(\infty)\rangle \tag{18}$$

Results and Discussion

Reactions R1 and R2 consist of potential wells with energies of 160.1 and 353.6 kJ mol^{-1}, respectively, lower than the value of total energies of the reactants at the CCSD(full)/Aug-cc-pVTZ level.[23] Potential energy barrier for reaction R3 is 30.1 or 79.4 kJ mol^{-1} at the G3 or CCSD(full) levels, respectively.[23] These values are corrected for zero-point energies. QCT calculations for three different channels R1, R2, and R3 on the lowest singlet potential energy surface were performed at five initial collision energy values from 6.3 up to 83.6 kJ mol^{-1}. The number of reactive trajectories N_r and reactive cross sections ($\sigma = \pi b^2_{max} P^r$) at different translational energies and vibrational states are listed in Table 2. In general, values of the calculated cross sections increase by increasing collision energy or the vibrational state of that particular bond that is being broken, although no significant changes in calculated cross sections was observed by increasing the collision energies from 62.7 to 83.6 kJ mol^{-1}.

To calculate the rate constants according to eq 7, values of σ as a function of temperature should be known. Maximum values of the impact parameters, reactive cross sections, and the number of effective trajectories as a function of initial translational temperature and initial vibrational quantum numbers of HO_2 for three different channels are listed in Table 3. As shown in Table 3, the effect of translational temperature on the reactive cross section from 300 to 600 K is more significant than its effect from 600 to 1200 K. As shown in Table 3, the calculated reactive cross sections for reactions R1 and R2 at 600 K are comparable with those values calculated at 1200 K. The effect of translational temperature and energy on the reactive cross section for reaction R3 is more important. Such a result should be reasonable due to the nature of reaction R3 that unlike reactions R1 and R2 proceeds through a barrier. Calculated rate constants according to eq 7 for three different channels as a function of σ and N_r at three different translational temperatures are also listed in Table 3.

Figures 2–4 show the dependence of the reactive cross sections for three different paths as a function of initial collision energy and initial vibrational state of HO_2. As shown in Figures 2–4, vibrational excitation of OO bond in HO_2 causes an increase in the reactive cross sections of reactions R1 and R2, where OO bond is broken. The reactive cross section of reaction R3 was affected by vibrational excitation of OH bond in HO_2 reactant.

In Figures 5–7 calculated rate constants from data in Table 3 and eq 7 for three channels R1, R2, and R3 in three different initial vibrational states of HO_2 are compared with experimental reported rate constants in the literature, respectively. The

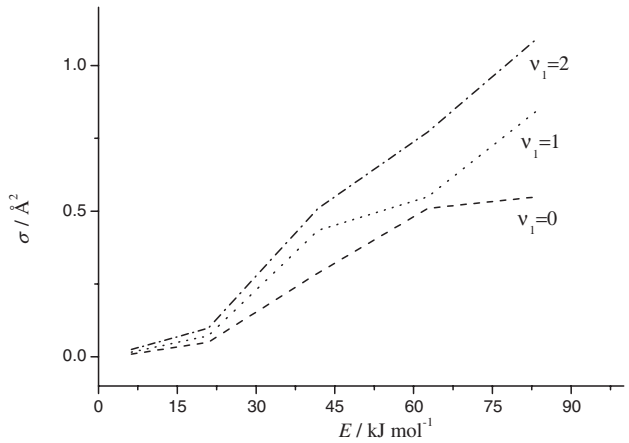

Figure 2. Reactive cross section for trajectories ending in $H_2O + O$ products (R1) as a function of collision energy and initial vibrational state of OO bond in HO_2 reactant.

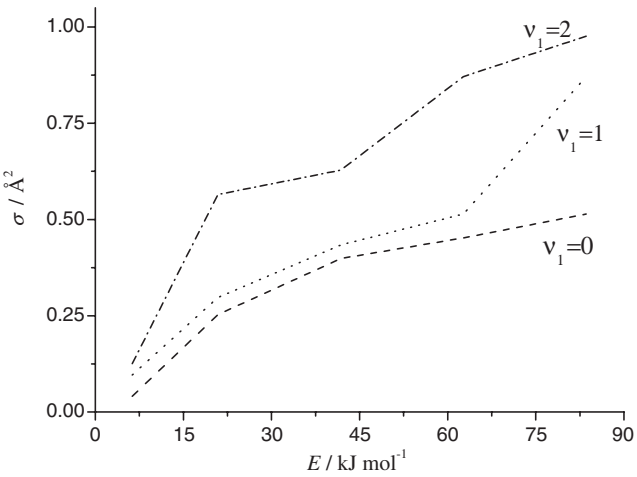

Figure 3. Reactive cross section for trajectories ending in 2OH product (R2) as a function of collision energy and initial vibrational state of OO bond in HO_2 reactant.

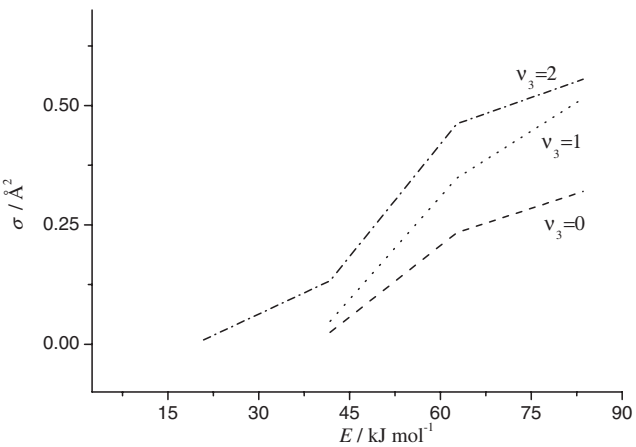

Figure 4. Reactive cross section for trajectories ending to $H_2 + O_2$ products (R3) as a function of collision energy and initial vibrational state of OH bond in HO_2 reactant.

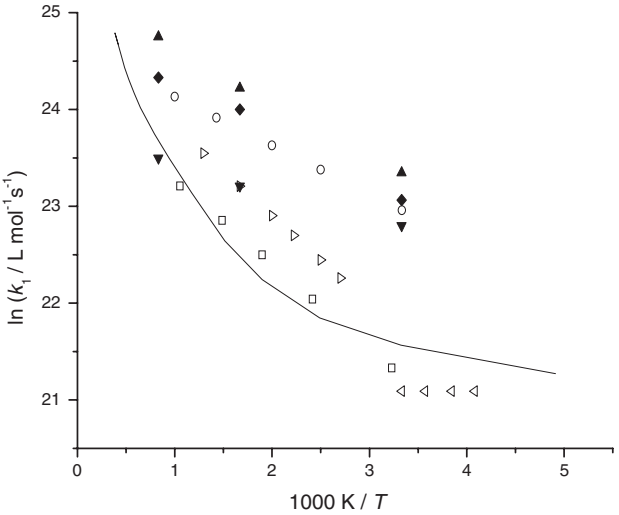

Figure 5. Arrhenius plot for reaction R1 to produce $H_2O + O$. (▼) Calculated at (000) vibrational level of HO_2, (◆) calculated at (100) vibrational level of HO_2, (▲) calculated at (200) vibrational level of HO_2, and solid line calculated at the CCSD(full) level from Ref. 23. Open symbols from experimental results as: (◁) from Ref. 11, (□) from Ref. 12, (▷) from Ref. 15, and (○) from Ref. 16.

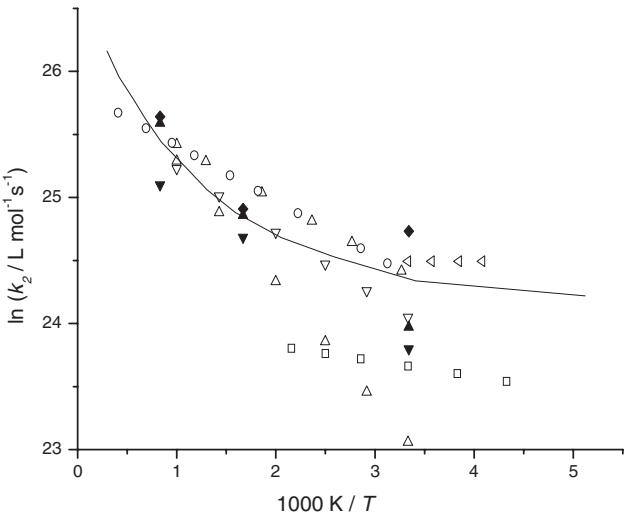

Figure 6. Arrhenius plot for reaction R2 to produce 2OH. (▼) Calculated at (000) vibrational level of HO_2, (▲) calculated at (100) vibrational level of HO_2, (◆) calculated at (200) vibrational level of HO_2, and solid line calculated at the CCSD(full) level from Ref. 23. Open symbols from experimental results for the formation of hydroxyl radical: (◁) from Ref. 11, (△) from Ref. 12, (○) from Ref. 14, (▽) from Ref. 17, (□) from Ref. 18, and (△) from Ref. 16.

data from references 11 and 12 in Figures 5–7 are evaluated from available kinetic data in the literature. Our results from the present work at lower vibrational states are in agreement with the available experimental data in the literature. For reaction R3, the calculated rate constant at different temperatures is compared with the reported experimental data for its equivalent reaction on the triplet surface (Scheme 4). To the best of our

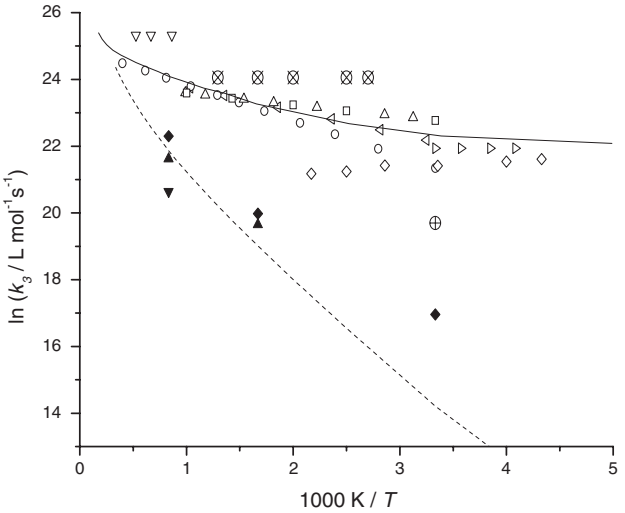

Figure 7. Arrhenius plot for reaction R3 to produce $O_2 + H_2$. (▼) Calculated at (000) vibrational level of HO_2, (▲) calculated at (001) vibrational level of HO_2, (◆) calculated at (002) vibrational level of HO_2, and solid line and dashed line calculated for reactions R5 and R3, respectively, from Ref. 23. Open symbols from experimental results as: (▷) from Ref. 11, (▽) from Ref. 13, (◁) from Ref. 12, (○) from Ref. 14, (△) from Ref. 17, (⊗) from Ref. 15, (□) from Ref. 16, (◇) from Ref. 18, and (⊕) from Ref. 6.

$$HO_2\ (^2A'')(\upsilon 00) + H(^2S) \rightarrow H_2(^1\Sigma_g^+) + O_2(^3\Sigma_g^-) \qquad \text{R5}$$

Scheme 4.

knowledge, no experimental data on the rate constant of reaction R3 is reported in the literature. Including the tunneling factor into the calculated rate constant for reaction R3 at 300 K according to G3 results caused an increase in the value of k_3 by a factor of 1.4 in natural logarithmic scale. As shown in Ref. 23, the calculated rate constant according to the transition state theory for reaction R3 is about 3000 times less than the calculated rate constant for reaction R5 at 300 K.

One of the interesting aspects about this system is the formation of two energized intermediates H_2OO^* and $HOOH^*$. Formation of these two intermediates occurs along with the allocation of some amount of energy into the newly formed O–H bond in each of these intermediates that makes them vibrationally excited. A detailed consideration of the dynamics of these intermediates, by monitoring the trajectories, reveals that water oxide and hydrogen peroxide like geometries largely undergo asymmetric or symmetric stretching like motions until they dissociate or stabilize by means of IVR. To illustrate the behavior of these two energized intermediates, the results of the two types of calculations regarding determination of the average lifetimes and IVR time constants will be presented here.

The reactive encounters for the formation of energized intermediates H_2OO^* and $HOOH^*$ were considered to calculate their average lifetimes $\langle\tau\rangle$.[30] The average lifetime at 1.5 and 20 kcal mol^{-1} translational energy was calculated from lifetime distribution according to

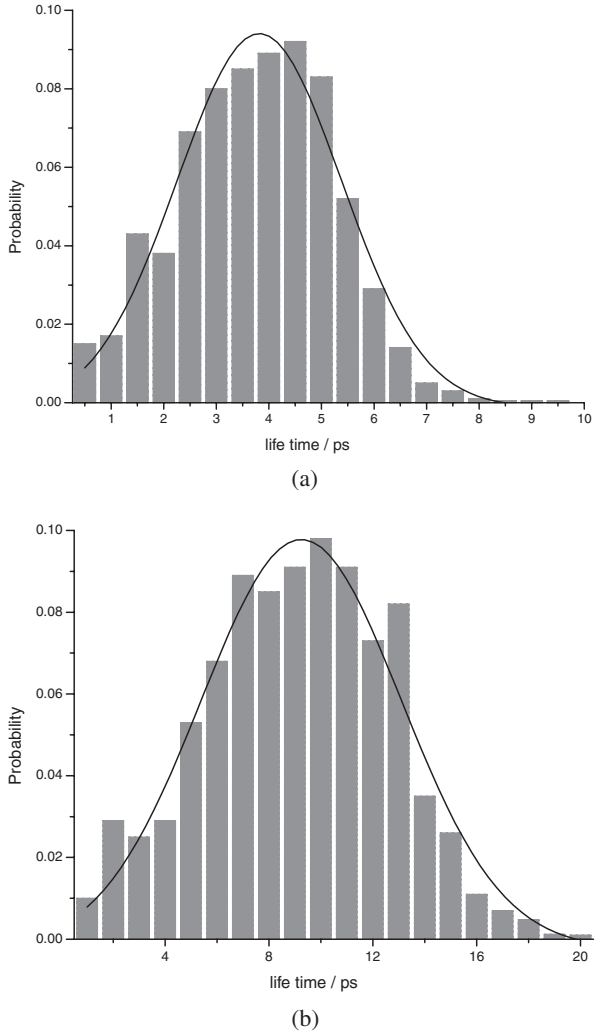

Figure 8. Calculated lifetime distributions for H_2OO^* (a) and $HOOH^*$ (b) at 6.3 kJ mol^{-1} translational energy.

$$\langle\tau\rangle = \sum_i \tau(N_i(\tau)/N_0) \qquad (19)$$

where the summation is over 200 trajectories (N_0) that were selected randomly from batches of 500 trajectories. Each trajectory was terminated when the separation between fragments of $HOOH^*$ or H_2OO^* was 3.5 Å. In measuring the lifetime, we have eliminated those encounters having lifetime less than 50 fs. The encounters for the formation of H_2OO^* complex had a value of $\langle\tau\rangle$ about 3.8 ps at 6.3 kJ mol^{-1} translational energy which decreased to a value of about 2.1 ps at 83.6 kJ mol^{-1} translational energy. The value of $\langle\tau\rangle$ for $HOOH^*$ intermediate was found to be about 9.3 ps at 6.3 kJ mol^{-1} translational energy that decreased to a value of about 5.4 ps at 83.6 kJ mol^{-1} translational energy. The calculated lifetime distributions at 6.3 kJ mol^{-1} for H_2OO^* and HOOH are shown in Figure 8. These average values of the lifetimes are valid in the absence of collisional deactivation. The collision frequency at 760 Torr is in an order of ca. 10^9 s^{-1}. The period of OO stretch in HOOH is about 38 fs and in H_2OO is about 30 fs. These values are much less than the calculated average lifetimes.

Table 4. Harmonic Vibrational Frequencies for HOOH

Mode	Assignment	Ab initio[a)]	Analytic potential	Experimental
ν_1	Torsion	384	442	371
ν_2	OO stretch	916	876	877
ν_3	Asym HOO bend	1310	1246	1266
ν_4	Sym HOO bend	1403	1415	1402
ν_5	OH sym stretch	3656	3663	3599
ν_6	OH asym stretch	3657	3666	3608

a) At the CCD/6-311+G(2d,2p) level.

To calculate the IVR time constants in HOOH, calculations were first carried out with initial vibrational energies in one of the OH modes corresponding to vibrational quantum levels from $\nu_{OH} = 2$ up to $\nu_{OH} = 6$. The same calculations were carried out with initial vibrational energies in the OO mode corresponding to vibrational quantum levels from $\nu_{OO} = 12$ up to $\nu_{OO} = 17$ in HOOH. This amount of energy ($\nu_{OO} = 17$) is necessary to cause dissociation of HOOH to 2OH.[23] Harmonic normal-mode frequencies for HOOH calculated from analytical potential are compared with those from ab initio calculations in Ref. 23 and experimental data[31] in Table 4. To examine the IVR time constant for OH bonds, at the beginning of each trajectory, the HOOH molecule excitation energy resides in one of the OH stretching modes. As time progresses, the excitation energy decays from the corresponding OH bond and is distributed among the other vibrational degrees of freedom. The results of $\langle E_{OH}(t)\rangle_{approx}$ corresponding to vibrational levels $\nu_{OH} = 2$, 4, and 6 are shown in Figure 9. The $\langle E_{OH}(t)\rangle_{approx}$ decays exponentially to a constant asymptotic value corresponds to the portion of the total vibrational energy that is statistically distributed in the corresponding OH stretching mode. We have noticed the coupling between the two OH stretches in hydrogen peroxide was very weak and the OH bonds exhibit local mode behavior in accordance with Ref. 32. The results of the same calculations for $\langle E_{OO}(t)\rangle_{approx}$ corresponding to vibrational levels $\nu_{OO} = 12$, 14, and 17 are shown in Figure 10. Our observations indicated that most of the energy in the OO bond distributed among the OOH bend and torsional modes in HOOH. In both cases, batches of 200 trajectories were calculated at the rotational temperature of $T_{rot} = 300$ K. The corresponding IVR time constants were obtained by a nonlinear least-squares fit of $\langle E_{OH}(t)\rangle_{approx}$ and $\langle E_{OO}(t)\rangle_{approx}$ to an exponential function. Equations 17 and 18 were fitted to the dynamic data points in Figures 9 and 10 for OH and OO bonds, respectively.

The fitted values for τ_{IVR} are summarized in Table 5. The IVR time constants τ_{IVR} decrease approximately exponentially with increasing initial excitation energy, consistent with Fermi's Golden Rule,[33] which predicts faster IVR decay at higher energies because of the higher vibrational state densities. The effect of rotation was investigated by changing the rotational temperature T_{rot} from 200 K up to 1200 K for OH and OO bonds in HOOH, where the results are shown in Table 6. Our results indicated that rotation has no meaningful effect on calculated IVR time constants τ_{IVR} within the dynamic calculations uncertainty of %95 confidence limit.

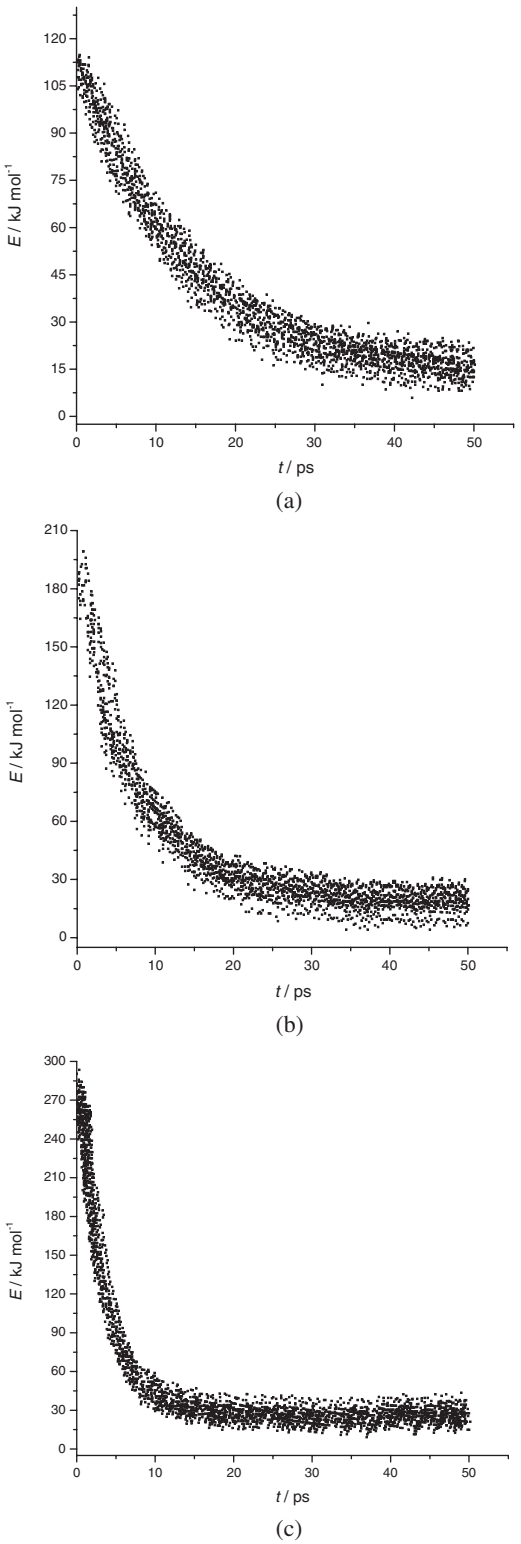

Figure 9. Decay of average energy in one of the OH stretching mode in HOOH at three different vibrational states $\nu = 2$ (a), $\nu = 4$ (b), and $\nu = 6$ (c) at $T_{rot} = 300$ K.

Conclusion

Results of QCT calculations for $HO_2 + H$ reaction on the lowest singlet potential energy surfaces are presented to examine the effect of formation of chemically activated

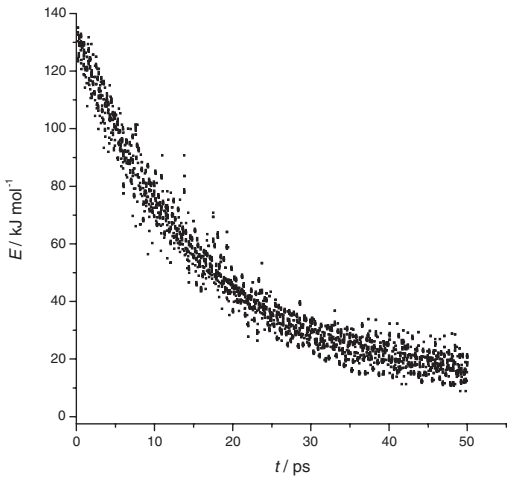

(a)

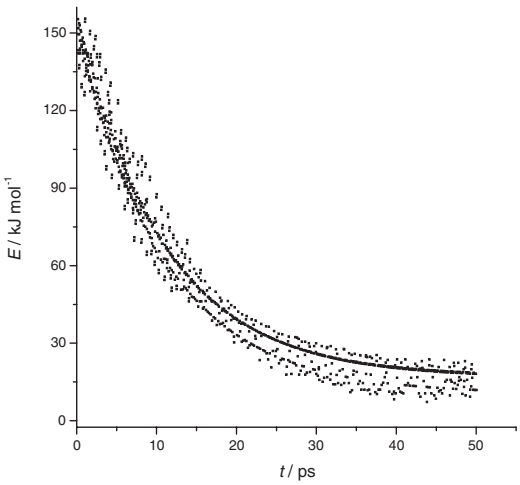

(b)

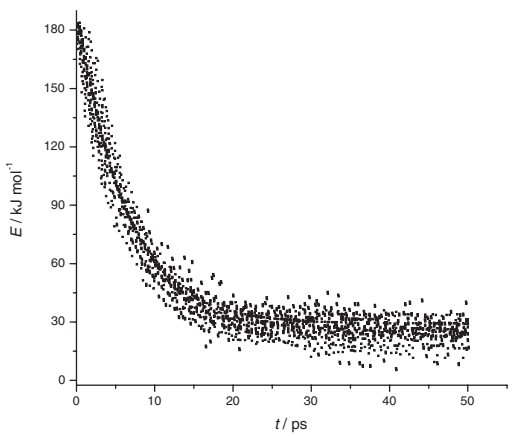

(c)

Figure 10. Decay of average energy in the OO stretching mode in HOOH at three different vibrational states $\nu = 12$ (a), $\nu = 14$ (b), and $\nu = 17$ (c) at $T_{rot} = 300$ K.

intermediates H_2OO^* and $HOOH^*$ on the rate of formation of the products. The theoretical results consisted of reaction probabilities as a function of translational energy and temperature, reactive cross sections, and initial reactant vibrational states. The calculated rate constants for different channels at lower vibrational states are reasonably close to the recommended experimental values except for reaction R3 for which no experimental data are available.

Table 5. Calculated IVR Time Constants at $T_{rot} = 300$ K in HOOH at $E_{tr} = 6.3$ kJ mol^{-1}

Initial vibrational level of O–H bond	τ_{OH}/ps	Initial vibrational level of O–O bond	τ_{OO}/ps
2	13.7	12	14.2
4	6.5	14	11.0
6	3.2	17	6.1

Table 6. IVR Time Constants for OH and OO Bonds in HOOH at Various Rotational Temperatures at $E_{tr} = 6.3$ kJ mol^{-1} and $\nu_{OH} = 2$ or $\nu_{OO} = 14$

T_{rot}/K	τ_{OH}/ps	τ_{OO}/ps
200	13.7	11.1
300	13.7	11.0
450	13.9	11.2
600	13.6	11.0
800	13.5	10.9
1000	13.6	11.1

The role of two potential wells in reactions R1 and R2 on the kinetics of this system is investigated. In both cases OO bond should be broken to form the relevant products, $H_2O + O$ in reaction R1 or 2OH in reaction R2, or one of the O–H bonds should be broken to form the reactants $HO_2 + H$. Our results indicated that calculated average lifetimes for both energized intermediates H_2OO^* and $HOOH^*$ are much longer than the corresponding vibrational time.

Quasi-classical trajectory simulations to measure the IVR time constants were carried out for HOOH molecule by monitoring the mean-square displacement of the OH or OO bonds as a function of time. In HOOH, the IVR time constants are predicted to decrease approximately exponentially with increasing initial energy. As shown in Table 6, rotational temperature has no effect on the IVR time constant.

As discussed in Ref. 27, two IVR time scales are at least involved in association reactions like formation of H_2OO^* and $HOOH^*$ in this system. The first time scale is governed by the rate of IVR between relatively isolated O–H stretch mode and the reservoir of remaining modes when the energized intermediates are forming. The second time scale is the time needed for the required energy to find its way back into the reaction coordinates (OH stretch mode or OO stretch mode) from the reservoir of other modes, to dissociate the newly formed H_2OO^* and $HOOH^*$ intermediates. If sufficient energy is not present in the reaction coordinates for dissociation into the reactants or products, these intermediates must live long enough for energy to find its way back into the reaction coordinates. In the present study we just calculated the first time scale for IVR reported in Table 5. We also calculated the lifetimes of the two newly formed intermediates H_2OO^* and $HOOH^*$. Our calculations for O–H or O–O stretch modes show the calculated IVR time constants are relatively close to the calculated lifetime for $HOOH^*$ intermediate. It should be

noticed that in our IVR and lifetime calculations we did not consider the collisions that causes energy-transfer processes. Therefore, more experimental and theoretical work is needed to decide whether statistical treatment for this system is applicable.

The support from the Research Council of Shiraz University is gratefully acknowledged.

References

1 D. R. Bates, M. Nicolet, *J. Geophys. Res.* **1950**, *55*, 301; I. C. McDade, E. J. Llewellyn, *J. Geophys. Res.* **1987**, *92*, 7643.

2 A. A. Westenberg, N. DeHaas, *J. Phys. Chem.* **1972**, *76*, 1586.

3 R. R. Baldwin, M. E. Fuller, J. S. Hillman, D. Jackson, R. W. Walker, *J. Chem. Soc., Faraday Trans. 1* **1974**, *70*, 635.

4 U. C. Sridharan, L. X. Qiu, F. Kaufman, *J. Phys. Chem.* **1982**, *86*, 4569.

5 L. F. Keyser, *J. Phys. Chem.* **1986**, *90*, 2994.

6 A. Boutalib, H. Cardy, C. Chevaldonnet, M. Chaillet, *Chem. Phys.* **1986**, *110*, 295.

7 S. P. Karkach, V. I. Osherov, *J. Chem. Phys.* **1999**, *110*, 11918.

8 A. L. Brunsvold, J. Zhang, H. P. Upadhyaya, T. K. Minton, J. P. Camden, J. T. Paci, G. C. Schatz, *J. Phys. Chem. A* **2007**, *111*, 10907.

9 a) R. D. Bach, A. L. Owensby, C. Gonzalez, H. B. Schlegel, *J. Am. Chem. Soc.* **1991**, *113*, 2338. b) R. D. Bach, A. L. Owensby, C. Gonzalez, H. B. Schlegel, J. J. W. McDouall, *J. Am. Chem. Soc.* **1991**, *113*, 6001. c) R. D. Bach, H. B. Schlegel, J. L. Andres, C. Sosa, *J. Am. Chem. Soc.* **1994**, *116*, 3475. d) R. D. Bach, M.-D. Su, *J. Am. Chem. Soc.* **1994**, *116*, 10103. e) J.-W. Chu, B. L. Trout, *J. Am. Chem. Soc.* **2004**, *126*, 900. f) D. Schröder, C. A. Schalley, H. Schwarz, N. Goldberg, J. Hrûsák, *Chem.—Eur. J.* **1996**, *2*, 1235. g) C. Meredith, T. P. Hamilton, H. F. Schaefer, III, *J. Phys. Chem.* **1992**, *96*, 9250. h) H. H. Huang, Y. Xie, H. F. Schaefer, III, *J. Phys. Chem.* **1996**, *100*, 6076. i) R. Sayós, C. Oliva, M. González, *J. Chem. Phys.* **2000**, *113*, 6736. j) M. Filatov, W. Reckien, S. D. Peyerimhoff, S. Shaik, *J. Phys. Chem. A* **2000**, *104*, 12014.

10 D. W. Toohey, J. G. Anderson, *J. Phys. Chem.* **1989**, *93*, 1049.

11 R. Atkinson, D. L. Baulch, R. A. Cox, R. F. Hampson, Jr., J. A. Kerr, M. J. Rossi, J. Troe, *J. Phys. Chem. Ref. Data* **1997**, *26*, 1329.

12 D. L. Baulch, C. J. Cobos, R. A. Cox, C. Esser, P. Frank, Th. Just, J. A. Kerr, M. J. Pilling, J. Troe, R. W. Walker, J. Warnatz, *J. Phys. Chem. Ref. Data* **1992**, *21*, 411.

13 Y. Hidaka, T. Taniguchi, H. Tanaka, T. Kamesawa, K. Inami, H. Kawano, *Combust. Flame* **1993**, *92*, 365.

14 W. Tsang, R. F. Hampson, *J. Phys. Chem. Ref. Data* **1986**, *15*, 1087.

15 R. R. Baldwin, R. W. Walker, *J. Chem. Soc., Faraday Trans. 1* **1979**, *75*, 140.

16 A. C. Lloyd, *Int. J. Chem. Kinet.* **1974**, *6*, 169.

17 J. Warnatz, in *Combustion Chemistry*, ed. by W. C. Gardiner, Jr., Springer-Verlag, NY, **1984**, p. 197.

18 G. L. Pratt, S. W. Wood, *J. Chem. Soc., Faraday Trans. 1* **1983**, *79*, 2597.

19 R. Shaw, *Int. J. Chem. Kinet.* **1977**, *9*, 929.

20 G. Dixon-Lewis, A. Williams, *Nature (London, U. K.)* **1962**, *196*, 1309; G. Dixon-Lewis, *Proc. R. Soc. London, Ser. A* **1970**, *317*, 235.

21 B. A. Thrush, J. P. T. Wilkinson, *Chem. Phys. Lett.* **1981**, *84*, 17.

22 W. Hack, A. W. Preuss, H. Gg. Wagner, K. Hoyermann, *Ber. Bunsen-Ges. Phys. Chem.* **1979**, *83*, 212.

23 S. H. Mousavipour, V. Saheb, *Bull. Chem. Soc. Jpn.* **2007**, *80*, 1901.

24 W. L. Hase, R. J. Duchovic, X. Hu, A. Komornicki, K. F. Lim, D.-H. Lu, G. H. Peslherbe, K. N. Swamy, S. R. V. Linde, A. Varandas, H. Wang, R. J. Wolf, *QCPE Bull.* **1996**, *16*, 43.

25 D.-H. Lu, W. L. Hase, R. J. Wolf, *J. Chem. Phys.* **1986**, *85*, 4422.

26 C. Doubleday, Jr., K. Bolton, G. H. Peslherbe, W. L. Hase, *J. Am. Chem. Soc.* **1996**, *118*, 9922.

27 Y. Liu, L. L. Lohr, J. R. Barker, *J. Phys. Chem. A* **2006**, *110*, 1267.

28 *NIST Computational Chemistry Comparison and Benchmark Database, NIST Standard Reference Database Number 101*, ed. by R. D. Johnson, III, **2006**, http://srdata.nist.gov/cccbdb.

29 Y. Liu, L. L. Lohr, J. R. Barker, *J. Phys. Chem. B* **2005**, *109*, 8304.

30 L. M. Yoder, J. R. Barker, *J. Phys. Chem. A* **2000**, *104*, 10184.

31 T. Shimanouchi, *Tables of Molecular Vibrational Frequencies*, *Consolidated Volume I (NSRDS NBS-39)*, American Chemical Society and the American Institute of Physics for the National Bureau of Standard, New York, **1972**, Consolidated Vol. I.

32 L. B. Harding, *J. Phys. Chem.* **1989**, *93*, 8004.

33 C. Cohen-Tannoudji, B. Diu, F. Laloe, *Quantum Mechanics*, Wiley, New York, **1977**, Vol. 2.